UDC 544.23.022, 544.478.02

DOI: 10.15372/CSD20202510

Morphology and Electrical Capacitance Properties of Nanostructured Composites PtM/Multi-Walled Carbon Nanotubes (M = Fe, Co)

YU. A. ZAKHAROV[1], G. YU. SIMENYUK[1], V. G. DODONOV[2], N. V. IVANOVA[2], A. A. LOBANOV[2], T. O. TROSNYANSKAYA[1], Z. R. ISMAGILOV[1]

[1]*Federal Research Centre of Coal and Coal Chemistry, Siberian Branch, Russian Academy of Sciences, Kemerovo, Russia*

[2]*Kemerovo State University, Kemerovo, Russia*

E-mail: galina-simenyuk@yandex.ru

(Received May 10, 2020)

Abstract

For the first time, nanocomposites based on non-ozonized and ozonized multi-walled carbon nanotubes (MWCNT) were obtained, with the outer and channel surfaces covered with nanosized crystallites of PtFe and PtCo bimetallic systems. The character of electrode Red-Ox processes taking place in a potential window from −1 to +1 V was established; electrochemical (energy storage) properties of nanocomposites in asymmetric two-electrode model cells of supercapacitors was studied. It was established that with an increase in the content of bimetallic phase up to 5 mass % in the composites, the electrode capacitance increases by a factor of 1.3–1.5 in comparison with initial nanotubes, which is explained by the formation of a pseudo-capacitive component due to the high-rate electrode Red-Ox processes involving intermetallic PtM.

Keywords: nanostructured composites, carbon nanotubes, bimetallic systems, supercapacitors, electrical capacitance

INTRODUCTION

One of the key problems in making competitive supercapacitors, with their short-term charging-discharging cycles and the possibility to generate high electric power as advantages over other electroaccumulating devices, is in the development of new electrode materials. Among the major directions of these developments, it is necessary to distinguish the formation of nanostructured composites (NSC) composed of carbon matrix containing the compounds of transition metals as fillers, undergoing Red-Ox transitions (desirably multiple) within the given potential window. Multi-walled carbon nanotubes (MWCNT) are usually used as the carbon matrix, and the metal-containing components of NSC are usually nano-sized oxides and hydroxides; the results of their investigation were published, for example, in [1–12].

Works dealing with the synthesis, investigation of the properties of carbon matrices filled with metals and the outlooks for their use as electrode materials of supercapacitors (SC) are almost absent because the advantages of SC are lost due to the low rates of the corresponding electrode Red-Ox reactions (the pseudo-capacitive component of total electric capacitance is formed and correspondingly discharged to the external circuit with a low rate).

Red-Ox processes providing pseudo-capacitance and participated by intermetallides appear to be more interesting and at the same time less studied. The most promising systems in this aspect include bimetals PtM (M = Fe, Co),

with their phase diagrams each containing three intermetallides with different component ratios, which implies the difference in Red-Ox potentials of their transformations in the potential window of ±1 V: MPt_3 (face-centred cubic (fcc) structure; space group *Pm*3*m* (221); structural prototype $CuAu_3$), MPt (tetragonal lattice, space group *P*4/*mmm*; structural prototype CuAu) and M_3Pt (fcc structure, space group *Pm*3*m*; structural prototype Cu_3Au).

The goal of the work was to study the formation of NSC PtM/MWCNT (M = Fe, Co), to investigate their morphology and electrochemical (electrocapacitance) properties, and to provide experimental confirmation of Red-Ox reactions proceeding with the participation of intermetallides.

EXPERIMENTAL

MWCNT synthesized at the Boreskov Institute of Catalysis, SB RAS (Novosibirsk) through pyrolysis of gas mixture (propane-butane) in the presence of nanoparticles of iron-containing catalysts were used as carbon matrices [13, 14]. The multiwall carbon nanotubes were treated preliminarily with a mixture of acids (HCl, HNO_3) to remove admixtures of catalysts. The major characteristics of MWCNT were established as a result of studies [4]: specific surface, 170 m^2/g; outer diameter of tubes, 17–22 nm; diameter of channels in tubes, 2–5 nm; wall thickness, 6–12 nm; MWCNT walls were formed from 4–12 graphene layers distinguished by means of a transmission electron microscope. To functionalize the surface, MWCNT were treated with ozone using an OGVK-02K ozonator (CC MELP, Russia). Ozonides (the intermediate products of ozone interaction with MWCNT) were destroyed by keeping the ozone-treated MWCNT at a temperature of 105 °C for 1 h.

Nanocomposites PtM/MWCNT (M = Fe, Co) were obtained through joint reduction of precursor solutions (hydrogen hexachloroplatinate(IV) and cobalt or iron chlorides, respectively) on MWCNT surface by sodium borohydride at room temperature. Metal phase content in the composites was 2.5 and 5 mass %, with the molar ratio Pt/M = 1 : 1.

The phase composition of NSC was studied by means of X-ray phase analysis (XPA) using X-ray diffractometer Difrey-401 (Russia, monochromatic FeK_α radiation, λ = 1.937 Å). The size distribution of nonuniformities was evaluated according to [15] relying on the data of small-angle X-ray scattering (SAXS) with the help of KRM-1 diffractometer (Russia). The electrical capacitance of nanocomposite electrodes was determined using a Parstat 4000A potentiostat (Princeton Applied Research, USA) within a potential window from −1 to +1 V, with potential scanning rates 10, 20, 40 and 80 mV/s. Measurements were carried out in two-electrode cells: a symmetrical one (for matrices) and asymmetrical (for composites, structures); the data processing procedure was described in [16, 17]. The nature of Red-Ox processes in NSC was studied by means of voltammetry using a Parstat 4000A potentiostat within the potential window from −1 to +1 V at the rate of potential scanning 10 mV/s.

RESULTS AND DISCUSSION

X-ray phase analysis

Figure 1 shows the diffraction patterns of MWCNT (non-ozonized (MWCNT-1) and ozonized (MWCNT-2) samples) and nanocomposites formed on the basis of these samples: PtCo/MWCNT-1, PtCo/MWCNT-2, PtFe/MWCNT-1, PtFe/MWCNT-2, containing the metal phase at a level of 2.5 and 5 mass %.

It is rather difficult to determine the phase composition and the size of crystallites of intermetallide nanoparticles from XPA data. In the diffraction patterns of PtCo/MWCNT NSC, over the background of the left shoulder of the reflection from the carbon matrix (2θ = 51–55°), a broad peak is observed at 45–52° with a notable maximum at 50.4° (over 2θ). At the right shoulder, maxima at 57° and 60° over 2θ may be distinguished. A qualitatively similar pattern of the structure of the major reflection of the matrix with the peaks detected at 50.4–50.5°, 56.9° and 60° over 2θ was also revealed in the diffraction patterns of PtFe/MWCNT.

According to the PDF database, reflections at 50° over 2θ are characteristic of platinum or its platinum-rich solid solutions with iron, cobalt with fcc structure; the group of reflections at larger angles (51–64° over 2θ) is characteristic of iron or intermetallides $PtFe_3$, PtFe, Pt_3Fe, $PtCo_3$, PtCo and Pt_3Co. It is difficult to make more distinct conclusions due to superpositions of reflections, low content and highly dispersed state of the metal-containing phase within the composite.

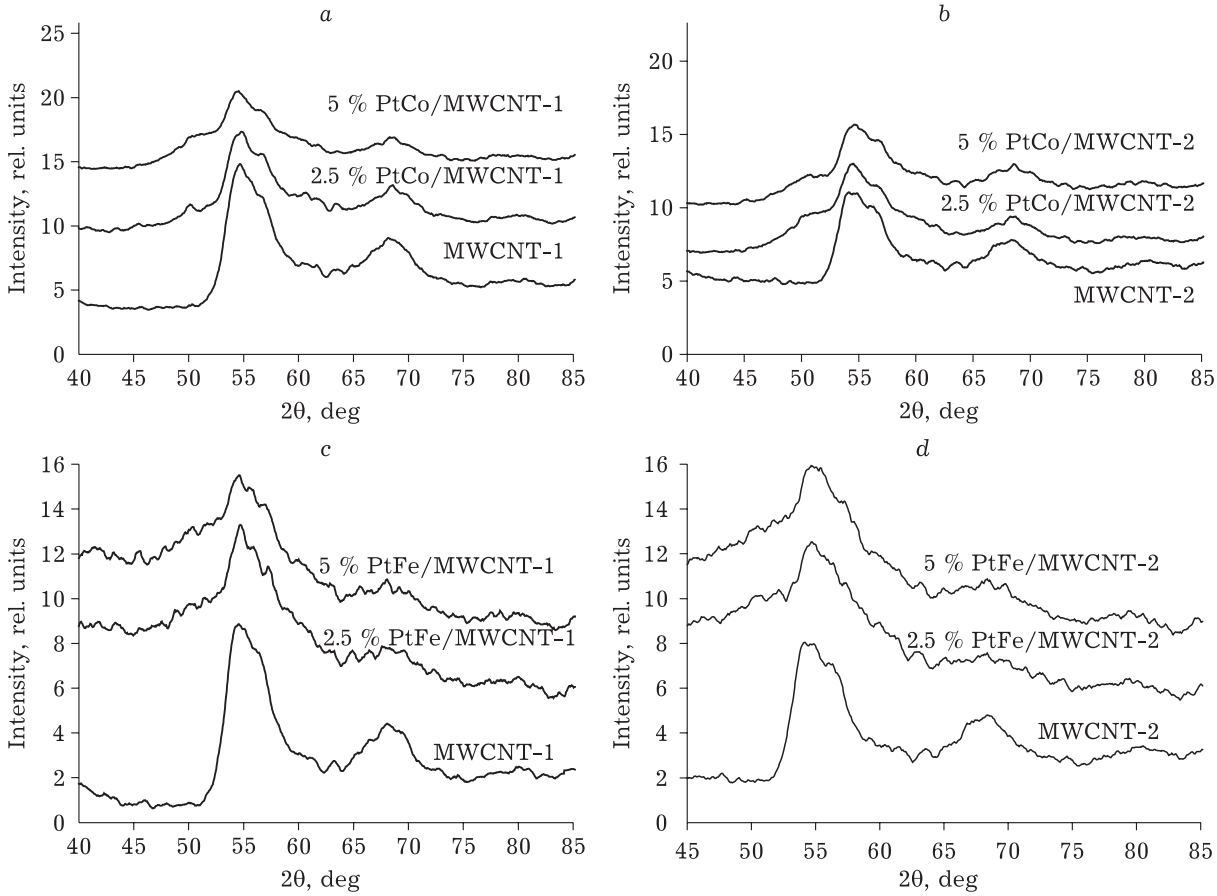

Fig. 1. Diffraction patterns of non-ozonized (MWCNT-1) (*a*, *c*) and ozonized (MWCNT-2) (*b*, *d*) samples of nanotubes and nanocomposites based on them (PtFe/MWCNT and PtCo/MWCNT) with different metal phase content.

X-ray fluorescence analysis

One can see in X-ray fluorescence spectra (Fig. 2) that initial carbon nanotubes MWCNT-1 and MWCNT-2, as well as NSC formed on their basis, contain insignificant amounts (0.1–0.2 mass %) of chlorine, calcium and chromium admixtures. This is the evidence of sufficiently high efficiency of sample purification at the stage of washing.

The intensities of X-ray fluorescence peaks related to platinum (9.4 keV) and cobalt (7.6 keV) change in proportion to the content of metal phases in NSC. Determination of iron content is hindered because the characteristic radiation of the iron anode of the X-ray tube is used for excitation.

Analysis of the size distribution of nonuniformities in the composites by means of SAXS

The experimental SAXS spectra of MWCNT samples of two kinds (MWCNT-1 and MWCNT-2) and NSC formed on their basis, as well as the functions of the size distribution of nonuniformities ($D_m(d)$) calculated from scattering curves and the difference functions ($\Delta D_m(d)$) are shown in Fig. 3.

For all the considered mode systems, maxima within the regions of 2–7 and 12–25 nm are clearly detected in the $D_m(d)$ plots. The correspondence of nonuniformity sizes (d) to the sizes of channels and outer diameters of MWCNT surely allows relating the observed nonuniformities exactly to them. This had to be expected from the theory of SAXS at the boundaries between media (phases) with different electron densities.

An increase in scattering intensity, observed on the $\Delta D_m(d)$ curves, is due to the deposition of bimetal nanoparticles both in channels and at the outer surface of MWCNT. This effect is due to the higher contrast of electron density at vacuum/bimetal and bimetal/carbon interfaces in NSC in comparison with the vacuum/carbon interface in MWCNT. A noticeable structure on $\Delta D_m(d)$ curves may be due to a more complicated profile of interphase boundaries in NSC (vacuum/bimetal/carbon/bimetal/vacuum).

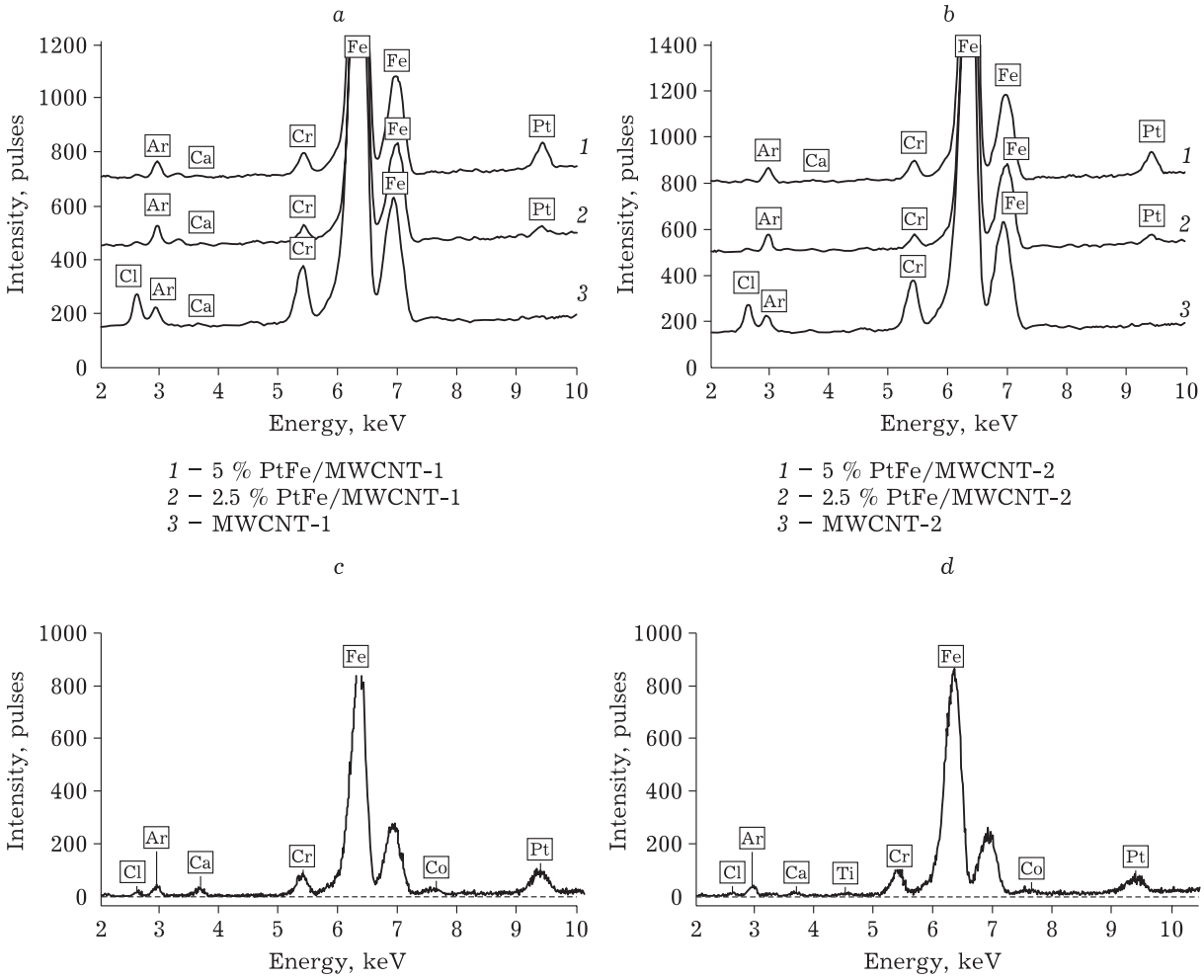

Fig. 2. X-ray fluorescence spectra of MWCNT and nanocomposites on their basis with different metal phase content: *a* – MWCNT-1 and PtFe/MWCNT-1; *b* – MWCNT-2 and PtFe/MWCNT-2; *c* – 5 % PtCo/MWCNT-1; *d* – 5 % PtCo/MWCNT-2.

In general, the data obtained by means of SAXS provide evidence of the formation of NSC as a result of the deposition of bimetal nanoparticles both in channels and on the outer surface of MWCNT.

Cyclic voltammetry of samples

The anode branches of cyclic voltammetric (CVA) curves for the PtFe bimetal films obtained by electrodeposition of precursor solutions are presented in Fig. 4 (*a*) in comparison with the nanopowders deposited on the electrode: PtFe (*b*) and PtCo (*c*). The conditions of the synthesis of bimetals by the reduction of precursors and their composition (Pt/M ratios) are similar to those used for the formation of bimetal fillers in NSC.

During the anode oxidation of electrodeposited bimetal films in the acid medium, three peaks are clearly detected on the CVA curves in the regions of about −0.4 V, −0.2 ... +0.3 V and near +0.6 V (see Fig. 4, *a*). Comparing these results with those obtained with nanopowders (see Fig. 4, *b*, *c*), one may conclude that the first peak, which is related to the iron-rich Pt–Fe solid solution on the basis of its position and the shift of the maximum with the changes in Pt/Fe ratio in the electrolyte, is characteristic only of electrodeposited systems. The nature of the second peak is known; it is connected with the electrocatalytic reduction of hydrogen in acid media on nanosized Pt-containing particles. Naturally, it does not appear in the alkaline medium used by us in the experiments on charge accumulation in model SC. The broad peaks detected in the region of +0.3 ...+0.8 V, judging from their position, relate to Red-Ox transformations participated by intermetallides Pt_3Fe (Pt_3Co) and maybe PtFe (PtCo).

Cyclic voltammetry with model supercapacitor cells

One can see in the massif of typical CVA curves shown in Fig. 5 that for non-ozonized

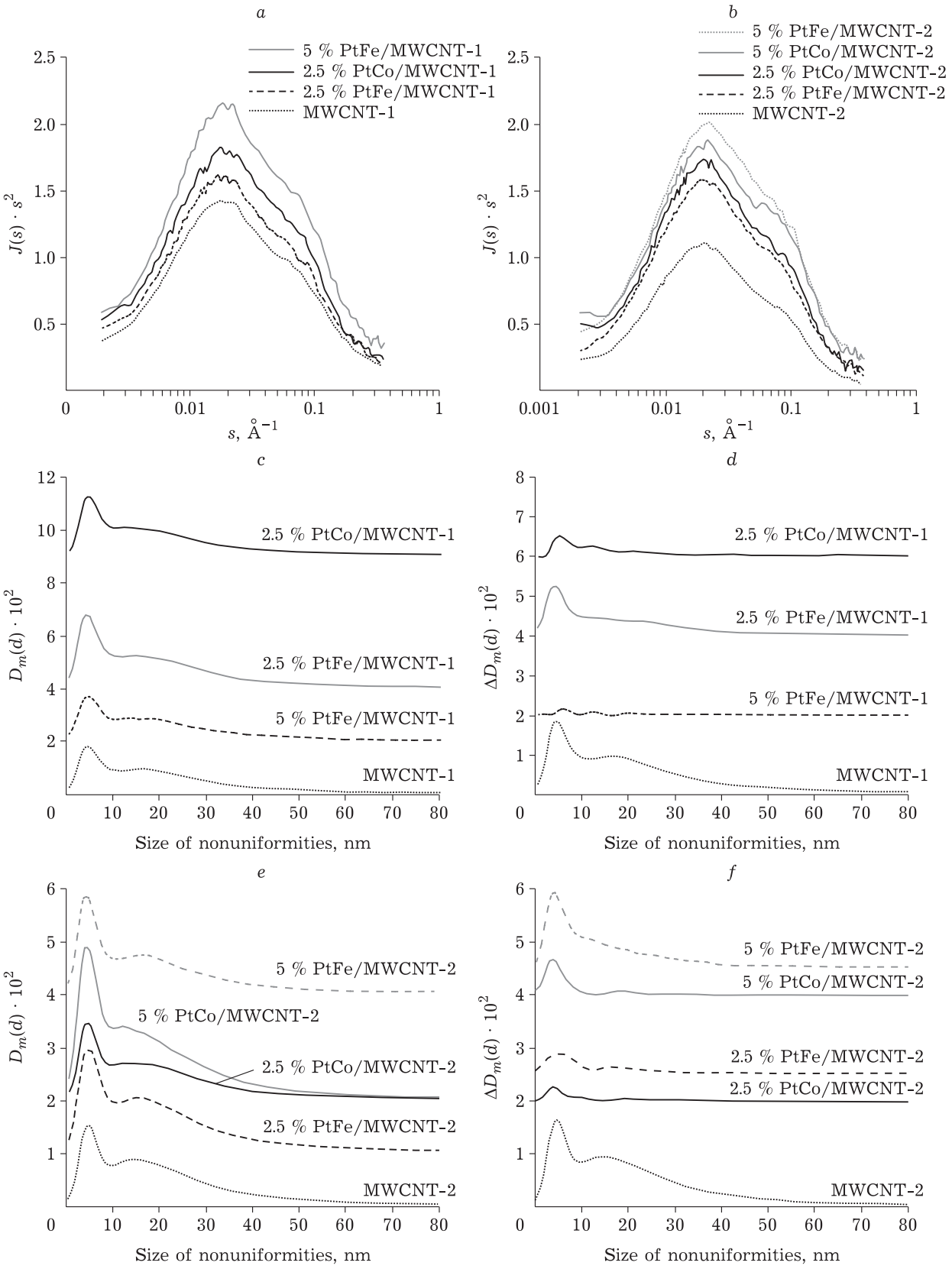

Fig. 3. Experimental SAXS curves of MWCNT-1 (non-ozonized) and MWCNT-2 (ozonized) samples and nanocomposites based on them (*a*, *b*), as well as calculated functions of nonuniformity size distribution (*c*, *e* – simple, *d*, *f* – difference functions).

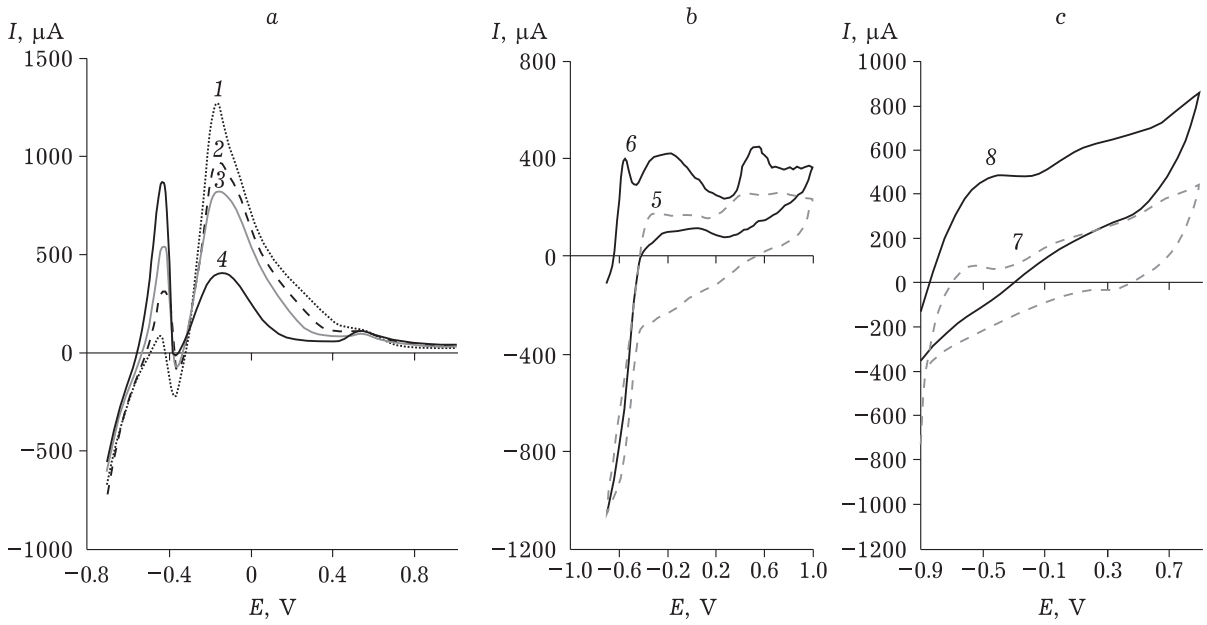

Fig. 4. Data of cyclic voltammetry: *a* – anode branches of CVA curves for electrolytic films PtFe, $c(PtCl_6^{2-}) = 6 \cdot 10^{-6}$ mol/L, $c(Fe^{2+})$, 10^{-5} mol/L: *1* – 4; *2* – 8; *3* – 16; *4* – 30; *b* – CVA curves for PtFe nanopowder; *c* – for PtCo nanopowder before (5, 7) and after (6, 8) cathode reduction. Conditions: *a*, *b* – electrolyte 0.1 M KCl + HCl (pH 1.65), *c* – ammonium buffer electrolyte (pH 9.8).

nanotubes (MWCNT-1) their shape is close to rectangular, therefore, charge accumulation occurs mainly at the boundary of the double electric layer (DEL) electrode/electrolyte.

For ozonized nanotubes (MWCNT-2), pseudo-capacitance peaks are observed on the discharge curve in the region of −0.8 V and on the charge curve (at +0.8 V), which are due to electrochemical Red-Ox reactions participated by oxygenated surface groups formed during functionalization (carboxyl, carbonyl, hydroxyl, *etc.*).

Pseudo-capacitive peaks that are observed on CVA curves in the case of electrodes made of NSC are likely to be connected with Red-Ox transformations of intermetallides. They are more clearly pronounced when the content of the bimetal filler is 5 mass %.

Cell capacities for different rates of potential scanning were determined from the area limited by CVA curves (Fig. 6). One can see that the capacitance of NSC electrodes is noticeably higher than the capacitance of MWCNT. The effect is more clearly pronounced for NSC based on ozonized nanotubes (MWCNT-2) containing 5 mass % PtCo.

In the region of relatively high potential scanning rates, the capacitance of MWCNT is only weakly dependent on the rate, but this dependence becomes more clearly expressed at lower rates (lower than 20–40 mV/s), and this effect is more notable for functionalized MWCNT-2. It follows from this observation that in the cases under consideration the accumulation of electric charge at high rates is connected mainly with the formation of the DEL; at low rates, the contribution of pseudo-capacitance becomes increasingly notable as a consequence of the involvement of Red-Ox electrochemical processes (for example, for MWCNT – with the participation of the surface groups, both the present ones and those formed during ozone treatment).

The studies showed [18–21] that intermetallides formed in nanosized PtFe and PtCo materials synthesized in the absence of MWCNT matrix are electrochemically active within the potential window from – 1 to +1 V. Red-Ox processes with their participation are likely to promote an increase in total electric capacitance. The presence of the effect in the region of high potential scanning rates provides evidence that the rates of these processes are substantial. An increase in the effect within the region of low scanning rates shows that several kinds of reactions proceeding with different rates are implemented.

Chronopotentiometric measurements

We carried out 100 cycles of cell charging-discharging, with each half-cycle lasting for 10 s,

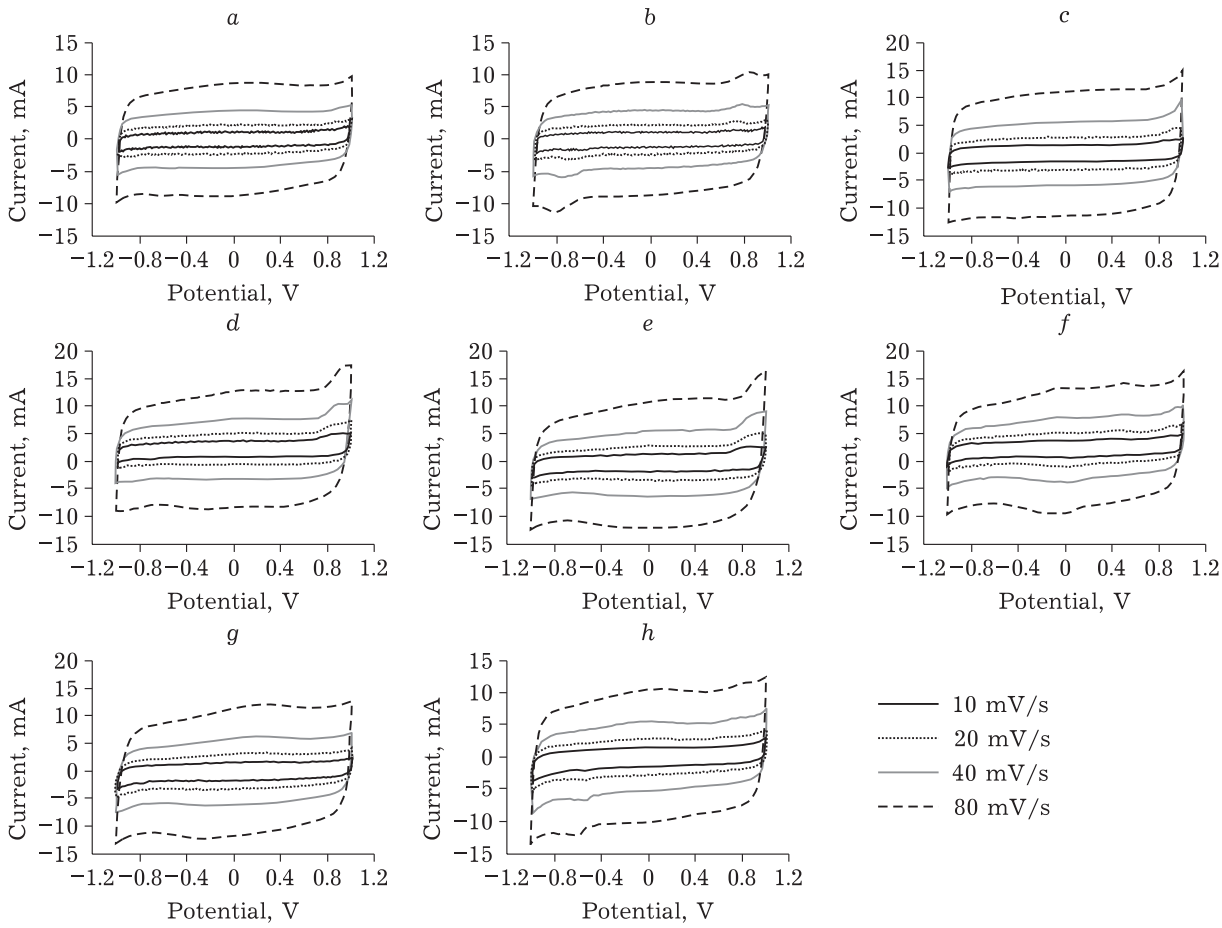

Fig. 5. CVA curves for symmetrical cells with electrodes based on non-ozonized MWCNT-1 (*a*) and ozonized MWCNT-2 (*b*) samples and asymmetrical supercapacitor cells with working electrodes based on nanocomposites: *c* – 2.5 % PtCo/MWCNT-1; *d* – 2.5 % PtCo/MWCNT-2; *e* – 5 % PtCo/MWCNT-1; *f* – 5 % PtCo/MWCNT-2; *g* – 5 % PtFe/MWCNT-1; *h* – 5 % PtFe/MWCNT-2. Conditions: counter-electrodes – MWCNT-1 or MWCNT-2; potential scanning rates, mV/s: 10 (*1*), 20 (*2*), 40 (*3*), 80 (*4*).

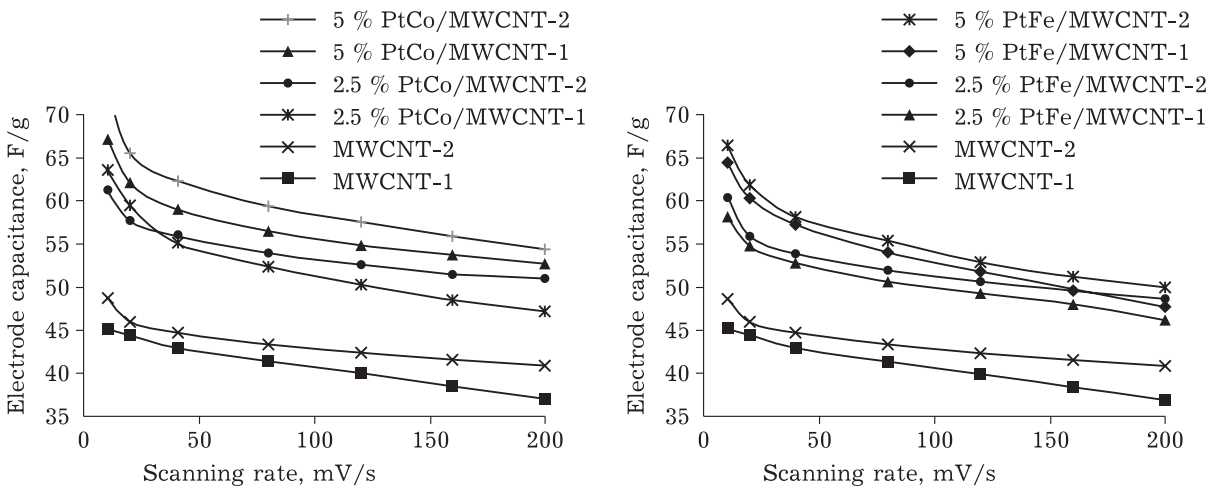

Fig. 6. Dependence of capacitance on potential scanning rate for cells with working electrodes based on MWCNT-1, MWCNT-2 and nanocomposites PtCo/MWCNT (*a*) and PtFe/MWCNT (*b*).

with the current equal to 10 mA. An example of the fragment of the cycle series is presented in Fig. 7.

The values of the calculated specific capacitance of electrodes and equivalent serial (internal) resistance of SC are presented in Table 1. One can see that the capacitance of composite electrodes is in all cases higher than that of the electrodes based on MWCNT. With an increase in the content of the metal phase in the composite, specific electric capacitance increases and the internal resistance of the cells decreases. At the qualitative level, the results correspond to the CVA data. The largest increase in capacitance is observed when the 5 % PtCo/MWCNT-2 nanocomposite is used as the working electrode of SC.

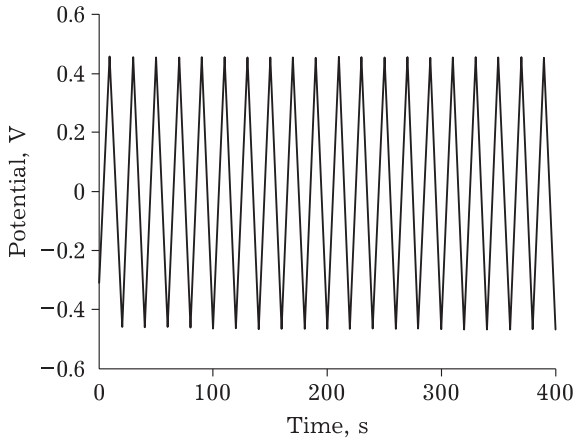

Fig. 7. Galvanostatic charging-discharging curves of supercapacitor cells with working electrode based on 5 % PtCo/MWCNT-2 nanocomposite.

TABLE 1

Specific electric capacitance of electrodes and internal resistance of SC cells

Sample	Specific electric capacitance, F/g	Internal resistance, Ohm
MWCNT-1	40.0	13.0
MWCNT-2	44.0	14.0
2.5 % PtCo/MWCNT-1	48.3	6.3
5 % PtCo/MWCNT-1	53.2	5.1
2.5 % PtCo/MWCNT-2	51.4	5.6
5 % PtCo/MWCNT-2	54.5	5.0
2.5 % PtFe/MWCNT-1	49.6	6.9
5 % PtFe/MWCNT-1	52.1	6.2
2.5 % PtFe/MWCNT-2	50.4	6.4
5 % PtFe/MWCNT-2	54.2	5.0

Electrochemical impedance spectroscopy

The data on the investigation of SC cells by means of impedance measurement are shown in Fig. 8. Measurements were carried out within a frequency range from $2.5 \cdot 10^{-2}$ to 104 Hz. One can see in Nyquist diagrams (see Fig. 8, a, b) that the introduction of the metal phase promotes a decrease in the active and reactive components of impedance. The active component exhibits a more substantial decrease (by a factor of 1.7–2), in particular, the resistance at the interface decreases in the same manner. This is due to the decoration of the surface of carbon nanotubes by nanosized quasi-films and nanocrystallites of bimetals having low specific resistance in comparison with MWCNT. At the same time, for cells with NSC electrodes, especially PtFe, an increase in the charge transfer resistance from 0.3–0.4 to 0.8–1.6 Ohm is observed (within the high-frequency range), which is inversely proportional to the rate of charge carrier transfer and is connected with kinetically hindered Red-Ox processes participated by intermetallides within the given potential window.

The dependences of the phase angle on frequency are shown in Fig. 8, *c*–*f*. One can see that the phase angle at low frequencies for the cells with MWCNT- and NSC-electrodes is 82–85°, which points to a substantial contribution of the DEL into charge accumulation. For an ideal SC, the angle is equal to 90°; for real cells with the electrodes accumulating energy mainly due to the DEL the angle is equal to 70–80°. In the region of high frequencies, corresponding to the region of charge transfer in Nyquist diagrams, maxima are observed for the cells with working electrodes based on NSC. Their intensity increases with an increase in the concentration of intermetallides, which points to the contribution from pseudo-capacitance. The most intense maxima were determined for PtFe systems.

CONCLUSION

Nanostructures composite materials PtM/MWCNT (M = Fe, Co) containing nanoparticles of PtM filler both in channels and on the outer surface of carbon matrix (MWCNT) were obtained for the first time. It was established that the developed composition and the structure of nanocomposite in combination with preliminary functionalization of MWCNT by means of treatment

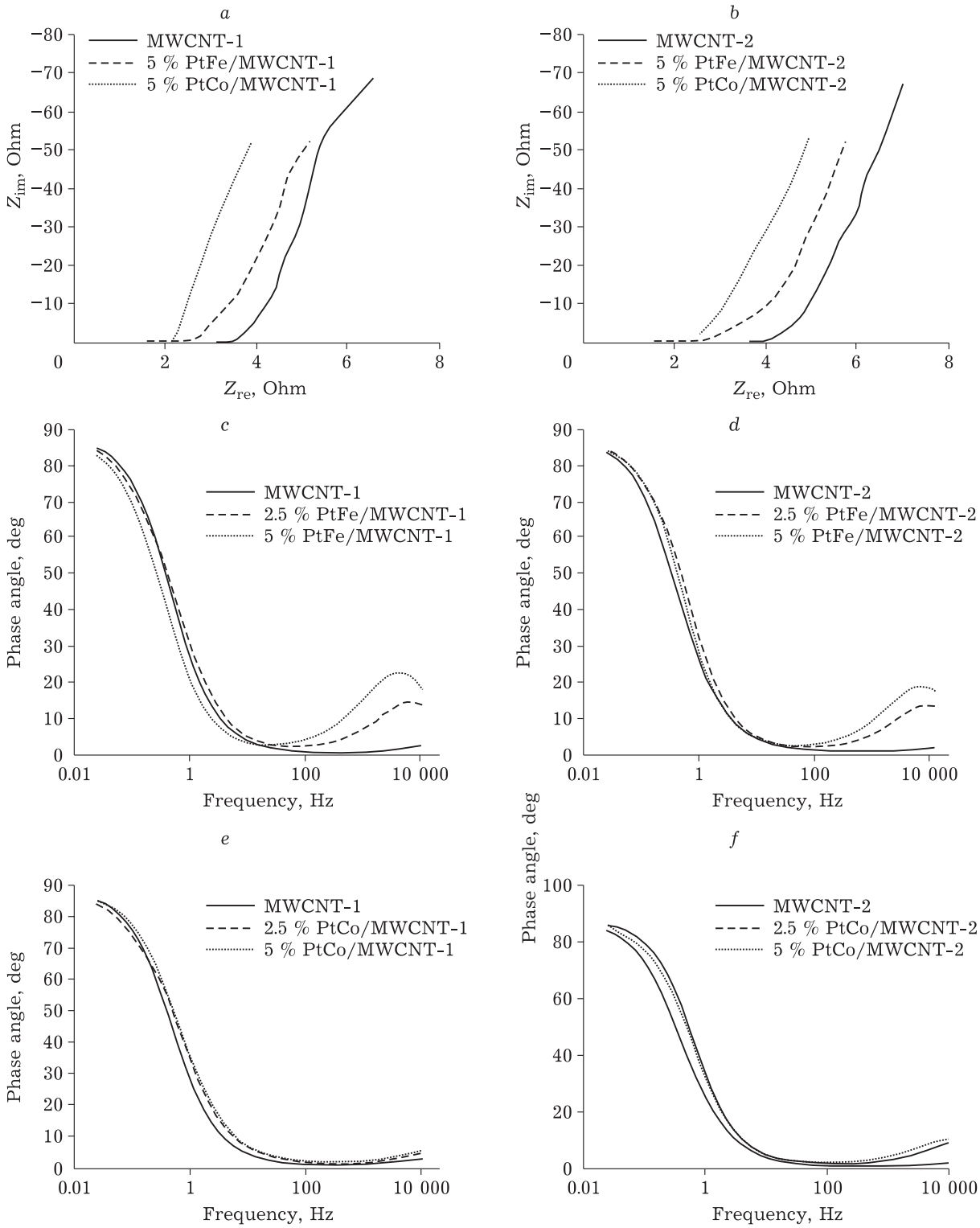

Fig. 8. Nyquist diagrams (*a*, *b*) and dependencies of phase angle on frequency (*c*–*f*) for supercapacitor cells with working electrodes: MWCNT-1 (*a*, *c*, *e*), MWCNT-2 (*b*, *d*, *f*) and nanocomposites based on them.

with ozone allow an increase in the electric capacitance of SC cells. This effect increases with an increase in the content of the bimetal filler. The largest effect (an increase in capacitance by a factor of 1.5) was achieved when the nanocomposite based on ozonized MWCNT containing 5 mass % PtCo was used as the material of the working electrode in the SC. The most probable

reason for the formation of an additional pseudocapacitive component in the composite may be fast electrode Re-Ox processes participated by PtM intermetallides.

The work was carried out with support from the Ministry of Education and Science (projects No. V.46.3.1, V.45.3.2) and RFBR (project No. 20-43-420017/20), using the equipment of the Shared Equipment Centre at the FRC CCC SB RAS.

Authors thank Cand Sci. in Technology A. S. Chichkan (IC SB RAS, Novosibirsk), Cand. Sci. in Chemistry E. S. Mikhailova (FRC CCC SB RAS, Kemerovo) for submitting the samples of multiwall carbon nanotubes.

REFERENCES

1 Kumar M. R. A., Abebe B., Nagaswarupa H. P., Murthy H. C. A., Ravikumar C. R., Sabir F. K., Enhanced photocatalytic and electrochemical performance of TiO_2-Fe_2O_3 nanocomposite: Its applications in dye decolorization and as supercapacitors, *Sci. Rep.*, 2020, Vol. 10, No. 1, P. 1249.

2 Podyacheva O. Yu., Stadnichenko A. I., Yashnik S. A., Stonkus O. A., Slavinskaya E. M., Boronin A. I., Puzynin A. V., Ismagilov Z. R., Catalytic and capacitance properties of nanocomposites based on cobalt oxide and nitrogen-doped carbon nanofibers, *Chin. J. Catal.*, 2014, Vol. 35, No. 6, P. 960–969.

3 Modafferi V., Triolo C., Fiore M., Palella A., Spadaro L., Pianta N., Ruffo R., Patanи S., Santangelo S., Musolino M. G., Effect of hematite doping with aliovalent impurities on the electrochemical performance of α-Fe_2O_3@rGO-based anodes in sodium-ion batteries, *Nanomaterials*, 2020, Vol. 10, No. 8, Article 1588, P. 1–18.

4 Zakharov Yu. A., Kachina E. V., Fedorova N. M., Larichev T. A., Simenyuk G. Yu., Pugachev V. M., Dodonov V. G., Zaytseva E. Yu., Yakubik D. G., Mikhaylova E. S., Morphology and electrochemical properties of nanostructured composite $Co_xNi_{(1-x)}$(OH)2/MWCNT based on carbon nanotubes, *Chemistry for Sustainable Development*, 2019, Vol. 27, No. 6, P. 590–597.

5 Han H., Sial Q. A., Kalanur S. S., Seo H., Binder assisted self-assembly of graphene oxide/Mn_2O_3 nanocomposite electrode on Ni foam for efficient supercapacitor application, *Ceramics International*, 2020, Vol. 46, No. 10, P. 15631–15637.

6 Liu S., Tan X., Zheng X., Liang S., He M., Liu J., Luo J., Zhang H., One-step microwave synthesis CoOOH/$Co(OH)_2$/CNT nanocomposite as superior electrode material for supercapacitors, *Ionics*, 2020, Vol. 26, No. 7, P. 3531–3542.

7 Larichev T. A., Fedorova N. M., Simenyuk G. Yu., Zakharov Yu. A., Pugachev V. M., Dodonov V. G., Yakubik D. G., Electrode material for supercapacitors based on carbon/nickel cobaltate nanocomposite synthesized by the thermal decomposition of cobalt and nickel azides, *Chemistry for Sustanable Development*, 2019, Vol. 27, No. 6, P. 610–617.

8 Moustafa H. M., Nassar M. M., Abdelkareem M. A., Mahmoud M. S., Obaid M., Synthesis of single and bimetallic oxide-doped rGO as a possible electrode for capacitive deionization, *J. Appl. Electrochem.*, 2020, Vol. 50, No. 7, P. 745–755.

9 Simenyuk G. Yu., Zakharov Yu. A., Kachina E. V., Pugachev V. M., Dodonov V. G., Gainutdinov A. R., Pomesyachnaya E. S., Influence of the conditions for obtaining nanocomposite electrode materials Mn_xO_y/MWCNT on their electrocapacitance characteristics, *Chemistry for Sustainable Development*, 2019, Vol. 27, No. 6, P. 633–642.

10 Cen D., Ding Y., Wei R., Huang X., Gao G., Wu G., Mei Y., Bao Z., Synthesis of metal oxide/carbon nanofibers via biostructure confinement as high-capacitance anode materials, *ACS Appl. Mater. Interfaces*, 2020, Vol. 12, No. 26, P. 29566–29574.

11 Wang S., Wang J., Ji X., Meng J., Sui Y., Wei F., Qi J., Meng Q., Ren Y., He Y., Zhuang D., Formation of hollow-cubic $Ni(OH)_2$/CuS_2 nanocomposite via sacrificial template method for high performance supercapacitors, *J. Mater. Sci.: Mater. Electron.*, 2020, Vol. 31, No. 13, P. 10489–10498.

12 Zakharov Yu. A., Pugachev V. M., Fedorova N. M., Dodonov V. G., Manina T. S., Ismagilov Z. R., Nanostructured C-Ni(OH)2-composites [in Russian], *Izv. Akad. Nauk. Ser. Khim.*, 2016, Vol. 65, No. 1, P. 120–124.

13 Svintsitskiy D. A., Kibis L. S., Smirnov D. A., Suboch A. N., Stonkus O. A., Podyacheva O. Yu., Boronin A. I., Ismagilov Z. R., Spectroscopic study of nitrogen distribution in N-doped carbon nanotubes and nanofibers synthesized by catalytic ethylene-ammonia decomposition, *Appl. Surf. Sci.*, 2018, Vol. 435, P. 1273–1284.

14 Chesnokov V. V., Chichkan A. S., Paukshtis E. A., Svintsitskiy D. A., Ismagilov Z. R., Parmon V. N., Modification of the surface of single-layered carbon nanotubes by functional nitrogen-containing groups and investigation of their properties [in Russian], *Dokl. Akad. Nauk*, 2017, Vol. 476, No. 5, P. 535–538.

15 Dodonov V. G., Zakharov Yu. A., Pugachev V. M., Vasilyeva O. V., Determination of the features of the structure of surface of nanosized metal particles according to the data of small angle X-ray scattering [in Russian], *Perspektivnye Materialy*, 2016, Vol. 7, No. 6, P. 68–82.

16 Simenyuk G. Yu., Zakharov Yu. A., Pavelko N. V., Dodonov V. G., Pugachev V. M., Puzynin A. V., Manina T. S., Barnakov Ch. N., Ismagilov Z. R., Highly porous carbon materials filled with gold and manganese oxide nanoparticles for electrochemical use, *Catal. Today*, 2015, Vol. 249, P. 220–227.

17 Simenyuk G. Y., Zakharov Y. A., Puzynin A. V., Barnakov Ch. N., Manina T. S., Ismagilov Z. R., Vladimirov A. A., Ivanova N. V., Pugachev V. M., Dodonov V. G., Ultrasonic assisted fabrication of nanocomposite electrode materials Au/C for low-voltage electronics, *Materials and Manufacturing Processes*, 2016, Vol. 31, No. 6, P. 739–744.

18 Kovács G., Kozlov S. M., Matolнnovб I., Vorokhta M., Matolín V., Neyman K. M., Revealing chemical ordering in Pt–Co nanoparticles using electronic structure calculations and X-ray photoelectron spectroscopy, *Phys. Chem. Chem. Phys.*, 2015, Vol. 17, P. 28298–28310.

19 Wellons M. S., Morris W. H., Gai Zh., Shen J., Bentley J., Wittig J. E., Lukehart Ch. M., Direct synthesis and size selection of ferromagnetic FePt nanoparticles, *Chem. Mater.*, 2007, Vol. 19, No. 10, P. 2483–2488.

20 Ivanova N., Lobanov A., Andyyakova A., Zakharov Yu., Popova A., Kolmykov R., The electrochemical synthesis and investigation of nanostructured Fe-Pt and Co-Pt systems, *IOP Conf. Ser.: Mater. Sci. Eng.*, 2020, Vol. 848, Article 012028. DOI: 10.1088/1757-899X/848/1/012028.

21 Ivanova N., The electrochemistry of intermetallic compounds: A mini-review, *Electrochem. Comm.*, 2017, Vol. 80, P. 48–54.